Article ID:0253-2778(2016)07-0557-10

New results on exotic baryon resonances at LHCb

ZHANG Liming (for the LHCb Collaboration)

(*Center for High Energy Physics, Tsinghua University, Beijing* 100084, *China*)

Abstract: Observation of exotic resonant structures decaying into $J/\psi p$ found in the LHCb experiment is discussed. Examination of the $J/\psi p$ system in $\Lambda_b^0 \to J/\psi K^- p$ decays shows two states, each of which must be composed of at least $c\bar{c}uud$ quarks, and are thus consistent with pentaquarks. The significance of each of these resonances is more than 9 standard deviations. Their masses are (4 380±8±29)MeV and (4 449.8±1.7±2.5)MeV, and their corresponding widths are (205±18±86)MeV, and (39±5±19)MeV. The preferred J^P assignments are of opposite parity, with one state having spin 3/2 and the other 5/2.

Key words: LHCb; exotic baryon; hidden-charmonium pentaquark

CLC number: O572.3 **Document code**: A doi:10.3969/j.issn.0253-2778.2016.07.004

Citation: ZHANG Liming. New results on exotic baryon resonances at LHCb[J]. Journal of University of Science and Technology of China, 2016,46(7):557-566.

LHCb 实验上新奇特重子的发现

张黎明(LHCb 合作组)

(清华大学高能物理研究中心,北京 100084)

摘要:介绍了 LHCb 实验上观测到的 $J/\psi p$ 奇特共振结构的实验证据.在 $\Lambda_b^0 \to J/\psi K^- p$ 衰变中,$J/\psi p$ 系统显示出两个共振态,每个至少含有五个夸克 $c\bar{c}uud$,和五夸克态相符.每个态的信号显著度都大于 9 倍的标准差.它们的质量为(4 380±8±29)MeV 和(4 449.8±1.7±2.5)MeV,对应的宽度为(205±18±86)MeV,和(39±5±19)MeV.最有可能自旋一个为 3/2,另一个为 5/2,宇称相反.

关键词:LHCb;奇特重子;隐形粲偶素五夸克态

0 Introduction

In 1964 Gell-Mann[1], and separately Zweig[2], proposed that hadrons were formed from fundamental point-like fractionally-charged objects now called quarks. The minimal quark configuration, that baryon is composed of three quarks and meson a quark and an anti-quark, can explain all well established hadrons for most of the last half-century. However, in the current decade there have been several observations of candidate mesonic states containing two quarks and two anti-quarks, called tetraquarks[3-4], and now, as described here, the observation of two pentaquark candidate baryon states[5]. Such multi-quark configuration were also discussed by the Gell-

Received:2015-11-30;**Revised**:2016-04-20

Foundation item:Supported by Funding of 1000 Young-Talented Plan in China.

Biography:ZHANG Liming, male, born in 1979, PhD/associate professor. Research field: high energy physics. E-mail: liming.zhang@cern.ch

Mann[1] and Zweig[2]. Several pentaquark observations made about ten years ago were all shown to be spurious[6]. Thus, the recent observation of two states decaying into $J/\psi p$, charmonium pentaquarks, found in $\Lambda_b^0 \to J/\psi K^- p$ decays by the LHCb experiment is surprising.

The Λ_b^0 decay mode was first observed by LHCb with an unexpected large yield and have been used to precisely measure the Λ_b^0 baryons lifetime[7-8]. However, one feature of the decay that was not addressed was an anomalous peaking structure in the $J/\psi p$ invariant mass spectrum, evident in the Dalitz plot shown in Fig. 1. While vertical bands correspond to $\Lambda^* \to K^- p$ resonances, shown by Feynman diagram in Fig. 2 (a), the horizontal band can only rise from structures in the $J/\psi p$ mass spectrum, by diagram in Fig. 2 (b). They can also be seen in the invariant mass projections shown in Fig. 3.

To claim such observations, we first addressed the two following questions: could the peak in the $J/\psi p$ mass distribution be caused by an experimental artifact or by an interference of various Λ^* amplitudes?

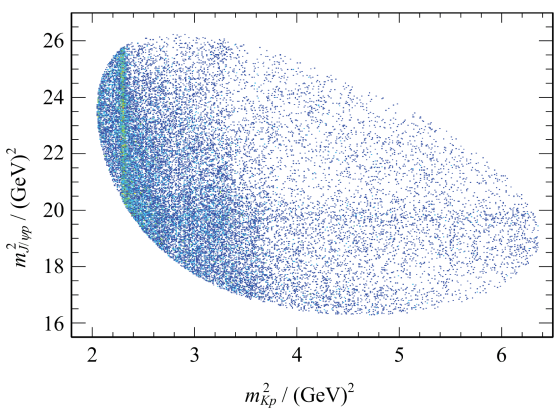

Fig. 1 Invariant mass squared of $K^- p$ versus $J/\psi p$ for candidates within ±15 MeV of the Λ_b^0 mass

1 Analysis and results

For this study LHCb[9] used data corresponding to 3 fb^{-1} of integrated luminosity in 7 and 8 TeV pp collisions. We reconstruct the $\Lambda_b^0 \to J/\psi K^- p$ decays by combining $J/\psi \to \mu^+ \mu^-$

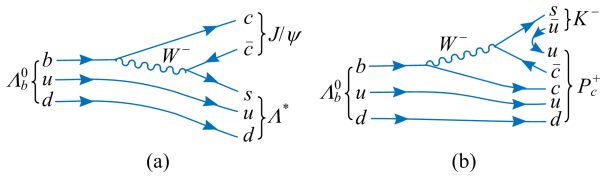

Fig. 2 Feynman diagrams for (a) $\Lambda_b^0 \to J/\psi \Lambda^*$ and (b) $\Lambda_b^0 \to P_c^+ K^-$ decay

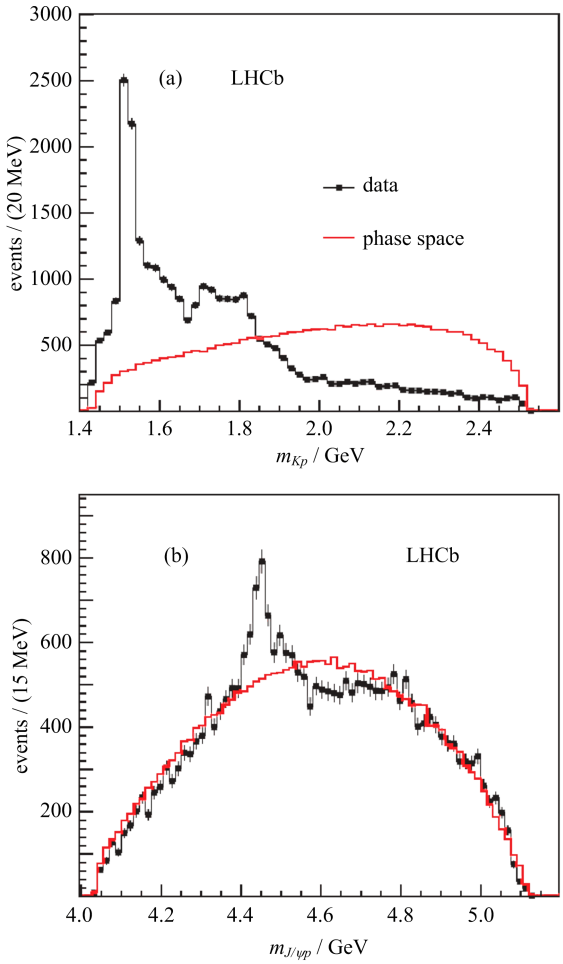

The solid (red) curve is the expectation from phase space. The background has been subtracted.

Fig. 3 Invariant mass of (a) $K^- p$ and (b) $J/\psi p$ combinations from $\Lambda_b^0 \to J/\psi K^- p$ decays

candidates with positive identified K^- and p tracks. The Λ_b^0 vertex is required to be well separated from the primary pp interaction vertex. A dedicated neutral network based selection criteria is optimized to achieve clean signals with high efficiency. The details are thoroughly described in Ref. [5]. In addition, specific backgrounds from $\overline{B}_s^0$ and $\overline{B}^0$ decays are vetoed

where the particle identification fails. We remove combinations that when interpreted as $J/\psi K^+K^-$ fall within ± 30 MeV of the $\overline{B}_s^0$ mass or when interpreted as $J/\psi K^-\pi^+$ fall within ± 30 MeV of the $\overline{B}^0$ mass. This requirement effectively eliminates background from these sources and causes only smooth changes in the detection efficiencies across the Λ_b^0 decay phase space. We have examined that potential backgrounds from Ξ_b decays cannot contribute significantly to our sample; these include Cabibbo-suppressed $\Xi_b^{-(0)} \to J/\psi K^- p\pi^{-(0)}$ and Cabibbo-favoured $\Xi_b^{-(0)} \to J/\psi K^- p K^-(\overline{K}^0)$. The resulting $J/\psi K^- p$ mass spectrum is shown in Fig. 4. There are $26\,007 \pm 166$ signal candidates containing 5.4% background within ± 15 MeV ($\pm 2\sigma$) of the $J/\psi K^- p$ mass peak. For subsequent analysis we constrain the $J/\psi K^- p$ four-vectors to give the Λ_b^0 invariant mass, J/ψ four-vectors to give the J/ψ mass and the Λ_b^0 momentum vector to be aligned with the measured direction from the primary to the Λ_b^0 vertices[10].

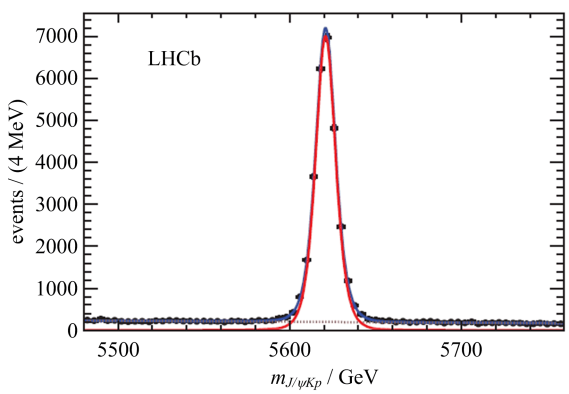

Fig. 4 Invariant mass spectrum of $J/\psi K^- p$ combinations, with the total fit, signal and background components shown as solid (blue), solid (red) and dashed lines, respectively

The overall detection efficiency determined from simulation and background from the sideband both smoothly vary across the Λ_b^0 decay phase space, and thus cannot generate such a narrow peak seen in the invariant mass of $J/\psi p$. In this sample specific tracking artifacts were looked for including fake tracks assembled from mismatched upstream and downstream segments, and multiple reconstructions of the same track. Having found no source of tracking artifacts, we proceeded to analyze the decay sequences represented by the Feynman diagrams shown in Fig. 2.

This requires a full analysis of the amplitude for each of the two decay sequences allowing for their mutual interference. The amplitudes are written using six independent variables; one is the invariant $K^- p$ mass, m_{Kp}, the others are decay angles. These are shown for the decay sequence $\Lambda_b^0 \to J/\psi\Lambda^*$, $\Lambda^* \to K^- p$, $J/\psi \to \mu^+\mu^-$ in Fig. 5. The Λ^* resonances are modeled by Breit-Wigner amplitudes except for the $\Lambda^*(1405)$ which is described by a Flatté function[11].

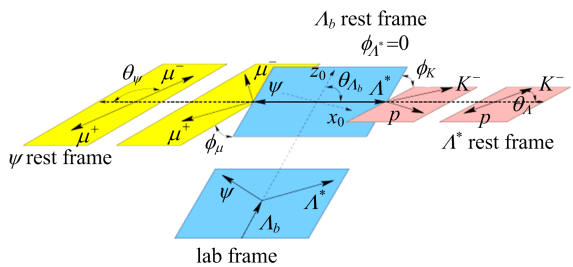

Fig. 5 Definition of the decay angles in the Λ^* decay chain

We first used the conventional resonances Λ^* and Σ^* to fit the data. We consider 14 Λ^* states. In each of their decays there are 4 or 6 independent LS (L is angular momenta and S total spin in Λ_b^0 decays) amplitudes that could be present. Not all of these states are likely to be produced in our final state and not all of the allowable decay angular momenta (LS couplings) are likely to be present. In order to make the most general description possible we first used all the possible states and decay angular momenta. Then data are fit to this model which has 146 free LS coupling coefficiencies, with the masses and widths of the resonant states fixed to their PDG values. Variations are considered later as part of the systematic uncertainties. The results of the fit are shown in Fig. 6. The fit gives a good description of the Λ^* states as can be seen in the m_{Kp} spectrum but fails to reproduce the structure in $m_{J/\psi p}$.

Several other different configurations were

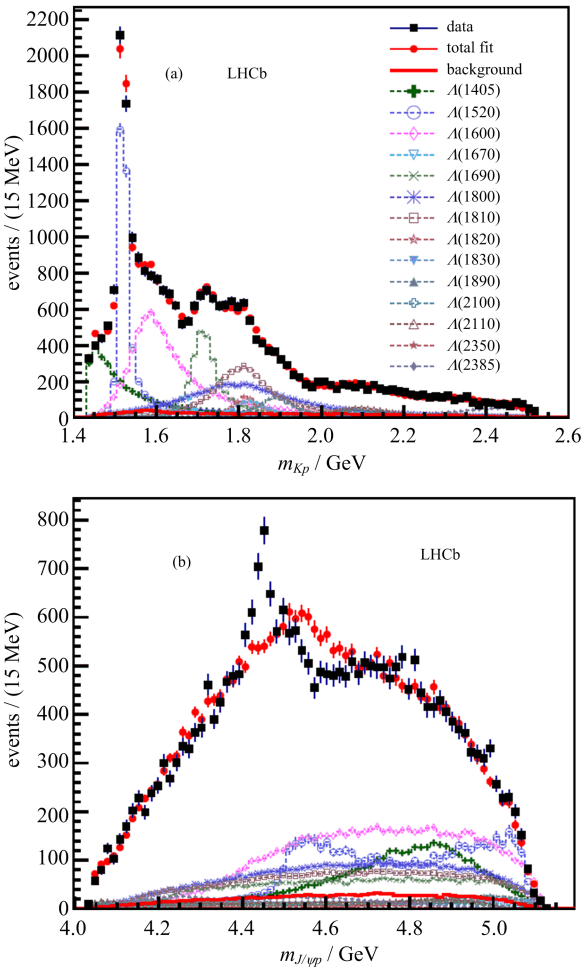

The data are shown as (black) squares with error bars, while the (red) circles show the results of the fit.

Fig. 6 Results for (a) m_{Kp} and (b) $m_{J/\psi p}$ for the extended Λ^* model fit without P_c^+ states

tried to improve the fit, but still none of these fits explains the data. These configurations are ① we added all the possible Σ^* states, ② we added two additional Λ^* allowing their masses and widths to float in the fit and allowed spins up to 5/2 with both parities, and ③ we added four non-resonant components with $J^P = 1/2^+$, $1/2^-$, $3/2^+$, and $3/2^-$.

Having failed to describe the data with conventional resources, we add one state decaying into $J/\psi p$. The matrix element for the decay sequence $\Lambda_b^0 \to P_c^+ K^-$, $P_c^+ \to J/\psi p$ is described by different mass and decay angles shown in Fig. 7. While these quantities can be expressed in terms of the used variables involving only Λ^* decays, thus do not provide additional fit variables. The detailed derivation of the matrix element is given in the arXiv article and the supplementary material for the Physical Review Letters publication[5].

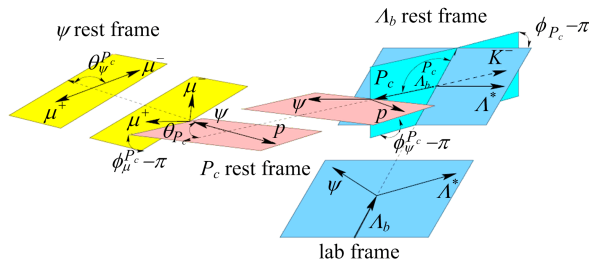

Fig. 7 Definition of the decay angles in the P_c^+ decay sequence

In each fit we minimize $-2\ln\mathscr{L}$ where $\mathscr{L}$ represents the fit likelihood. The $\Delta(-2\ln\mathscr{L})$ between different amplitude models allows to discriminate the models. A preferred model gives the smallest $-2\ln\mathscr{L}$. Separate fits for J^P values of $1/2^\pm$, $3/2^\pm$, $5/2^\pm$ and $7/2^\pm$ were tried. We allowed the mass and width of the putative P_c^+ state to vary. The best fit prefers a $5/2^+$ state, which reduces $-2\ln\mathscr{L}$ by 215. Fig. 8 shows the projections for this fit. Even though the m_{Kp} projection is well described, clear discrepancies in $m_{J/\psi p}$ remain visible.

To improve the fit, a second P_c^+ was added. These fits were performed both with the reduced model and the extended model in order to estimate systematic uncertainties. The best fit projections are shown in Fig. 9. Both m_{Kp} and the peaking structure in $m_{J/\psi p}$ are reproduced by the fit. The reduced model has 64 free parameters for the Λ^* rather than 146 and allows for a much more efficient examination of the parameter uncertainties and, thus, is used for numerical results. The two P_c^+ states are found to have masses of $(4\,380\pm8\pm29)$ MeV and $(4\,449.8\pm1.7\pm2.5)$ MeV, with corresponding widths of $(205\pm18\pm86)$ MeV and $(39\pm5\pm19)$ MeV, and called $P_c(4380)^+$ and $P_c(4450)^+$. Whenever two uncertainties are

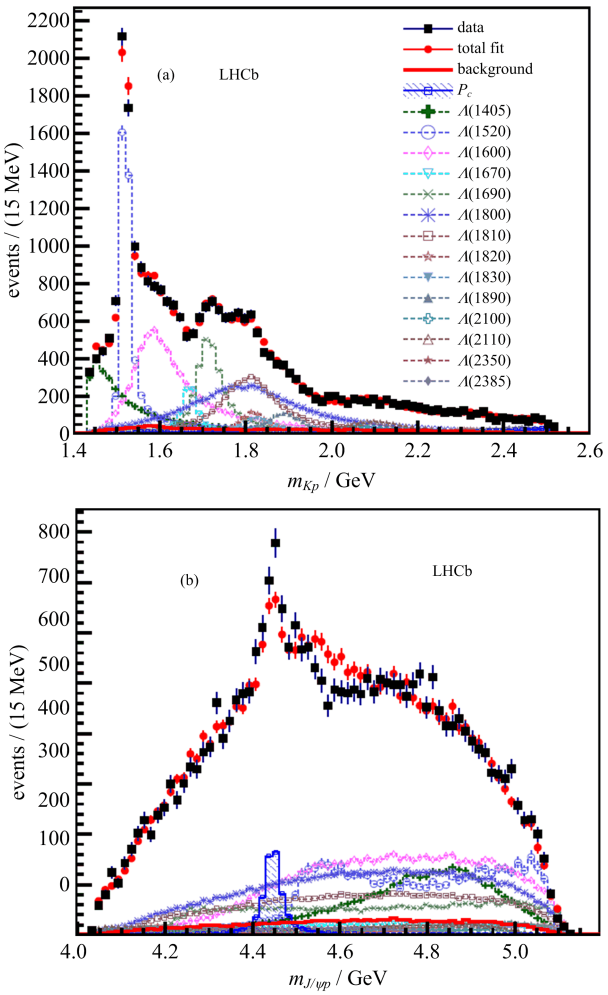

Fig. 8 Results of the fit with one $J^P = 5/2^+$ P_c^+ candidate

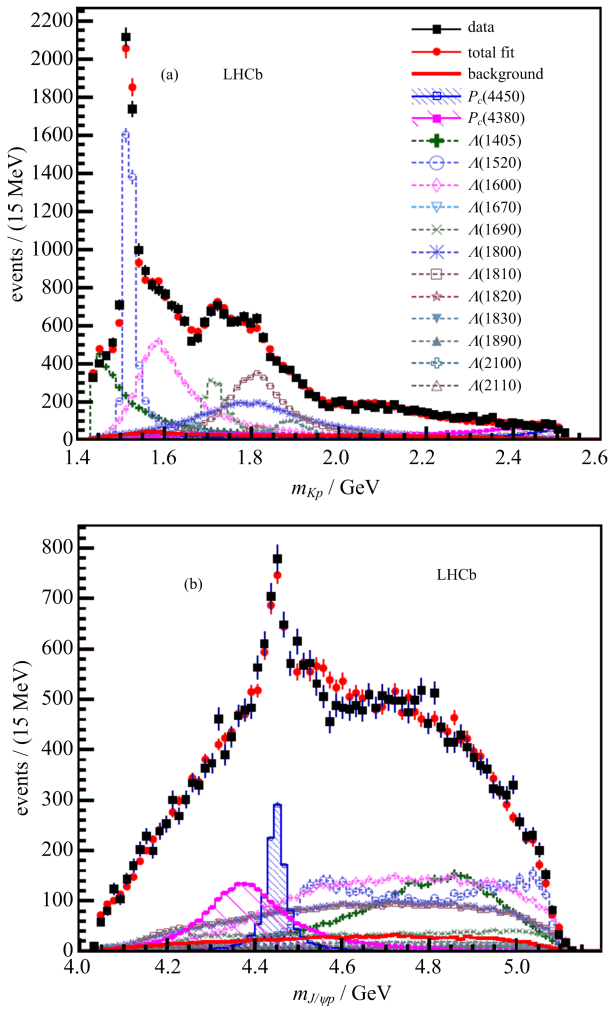

Fig. 9 Results of the fit using the reduced Λ^* model with two P_c^+ states

quoted the first is statistical and the second systematic. The fractions of the total sample due to the lower mass and higher mass states are $(8.4 \pm 0.7 \pm 4.2)\%$ and $(4.1 \pm 0.5 \pm 1.1)\%$, respectively. The overall branching fraction has recently be determined to be[13]

$$\mathcal{B}(\Lambda_b^0 \to J/\psi K^- p) = (3.04 \pm 0.04^{+0.55}_{-0.43}) \times 10^{-4} \tag{1}$$

where the systematic uncertainty is largely due to the normalization procedure, leading to the product branching fractions:

$$\left.\begin{aligned}\mathcal{B}(\Lambda_b^0 \to P_c(4380)^+ K^- p)\mathcal{B}(P_c(4380)^+ \to J/\psi p) = \\ (2.56^{+1.38}_{-1.34}) \times 10^{-5} \\ \mathcal{B}(\Lambda_b^0 \to P_c(4450)^+ K^- p)\mathcal{B}(P_c(4450)^+ \to J/\psi p) = \\ (1.25^{+0.42}_{-0.40}) \times 10^{-5}\end{aligned}\right\} \tag{2}$$

where all the uncertainties have been added in quadrature. Toy simulations are done to more accurately evaluate the statistical significances of the two states, resulting in 9 and 12 standard deviations, for lower mass and higher mass states, using the extended model which gives lower significances to account for systematic uncertainties.

The best fit has spin-parity J^P values of $(3/2^-, 5/2^+)$ for low and high mass states. Acceptable solutions are also found for additional cases with opposite parity, either $(3/2^+, 5/2^-)$ or $(5/2^+, 3/2^-)$. The five angular distributions are also well described by the fit shown in Fig. 10.

The fit projections in different slices of $K^- p$

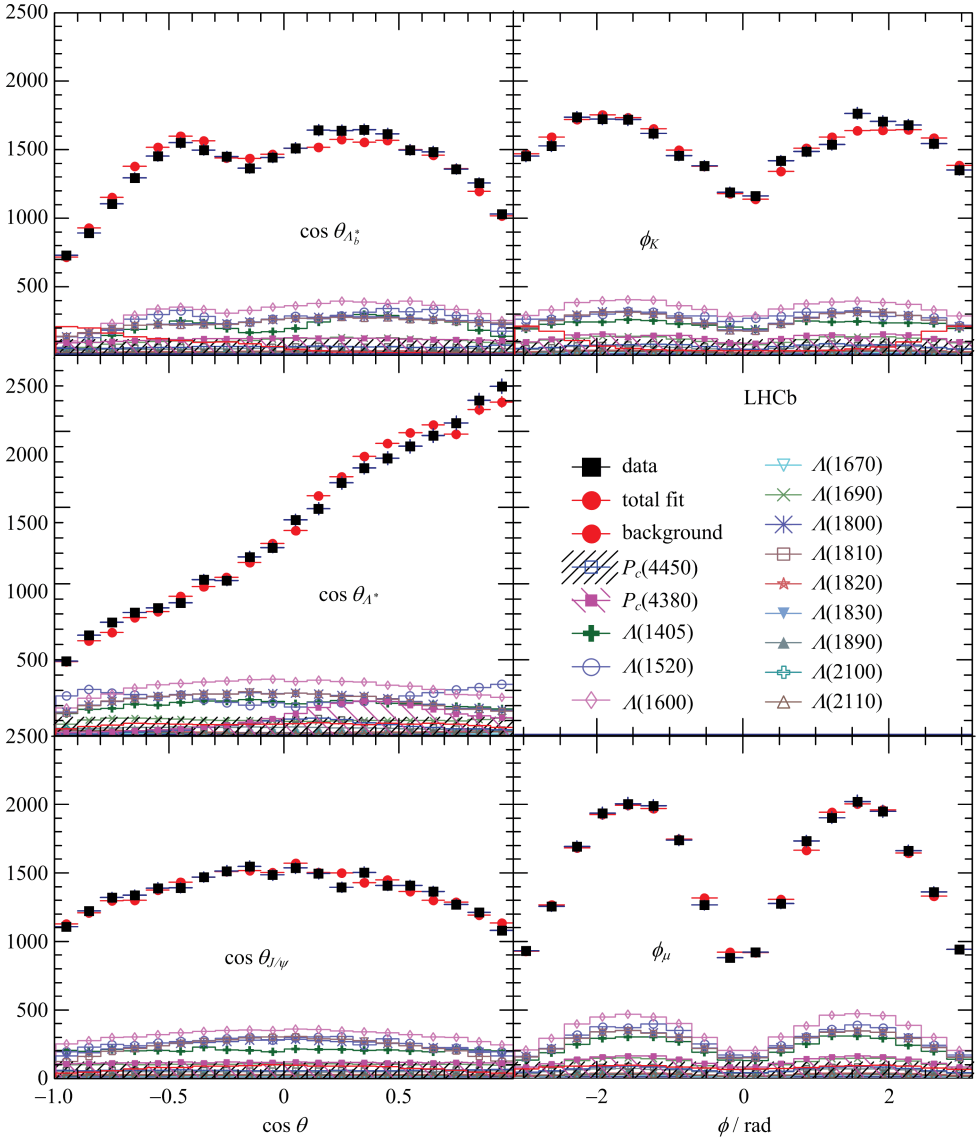

The data are shown as (black) squares, while the (red) circles show the results of the fit. Each fit component is also shown.

Fig. 10 Various decay angular distributions for the fit with two P_c^+ states

invariant mass are given in Fig. 11. In slice (a) the P_c^+ states are not present, as they are outside of the kinematic boundary. In slice (d) both P_c^+ states form a large part of the mass spectrum; there is also a considerable amount of negative interference between them. This can be seen better by examining the helicity angle of the P_c^+, θ_{P_c}, defined in Fig. 7. The efficiency corrected and background subtracted fit projection of the decay angular distribution is shown in Fig. 12 for the entire m_{Kp} range. The summed fit projection agrees very well with the angular distribution in the data, showing that two interfering states are needed to reproduce the asymmetric distribution. It is also shown mathematically that the two states need to be of opposite parity to produce such asymmetric distribution.

Systematic uncertainties are evaluated. The largest contribution comes from Λ^* modeling including the extended versus reduced model, varying the Λ^* masses and widths, and inclusion of a nonresonant amplitude in the fit. Sizable

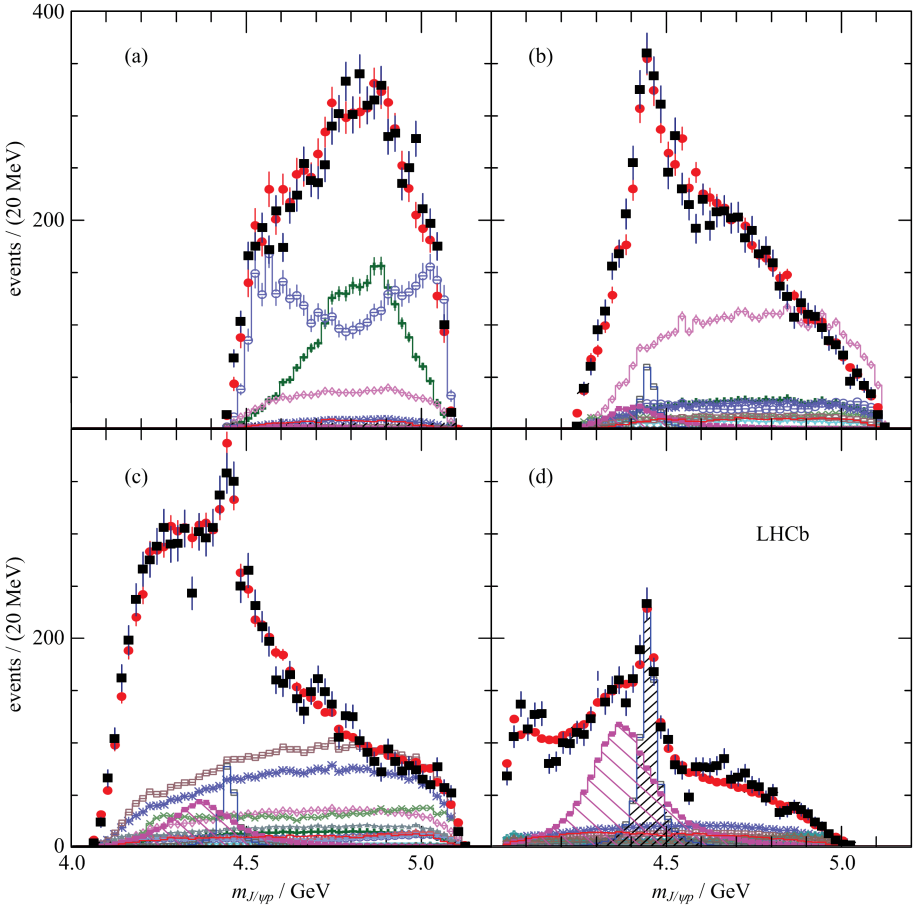

The data are shown as (black) squares with error bars, while the (red) circles show the results of the fit. The blue and purple histograms show the two P_c^+ states. See Fig. 10 for the legend.

Fig. 11 $m_{J/\psi p}$ **in various intervals of** m_{Kp} **for the fit with two** P_c^+ **states: (a)** m_{Kp} **<1.55 GeV, (b) 1.55 GeV<** m_{Kp} **<1.70 GeV, (c) 1.70 GeV<** m_{Kp} **<2.00 GeV, and (d)** m_{Kp} **>2.00 GeV**

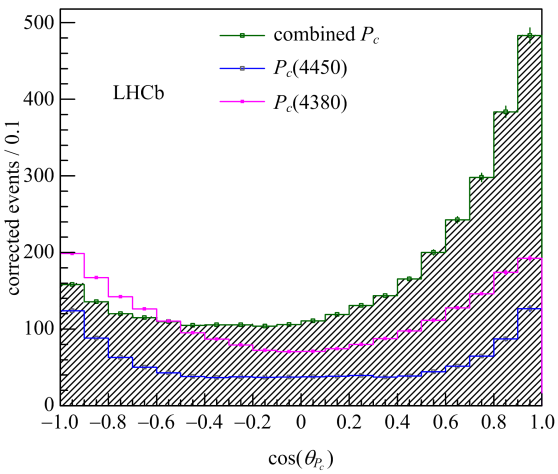

Values of $\cos\theta_{P_c}$ near −1 are correlated with values of m_{Kp} near threshold, while those near +1 are correlated with higher values.

Fig. 12 Efficiency corrected and background subtracted fit projections of the decay angular distributions for the two P_c^+ **states and their sum**

uncertainties are obtained for alternate J^P fits, varying the Blatt-Weisskopf barrier factor and changing the angular momentum L by one or two units. A nonresonant P_c^+ was also included and gave small systematic uncertainty. Consistent results are obtained from two fitters using different methods to account for the background, called "sFit" and "cFit" provided by two institutes.

The stability of the results is cross-checked by comparing the data recorded in 2011/2012, with the LHCb dipole magnet polarity in up/down configurations, $\Lambda_b^0/\overline{\Lambda}_b^0$ decays, and Λ_b^0 produced with low/high values of p_T. The fitters were tested on simulated pseudoexperiments and no biases were found. In addition, selection

requirements are varied, and the vetoes of $\overline{B}_s^0$ and $\overline{B}^0$ are removed and explicit models of those backgrounds added to the fit; all give consistent results.

Further evidence for the resonant character of the higher mass, narrower, P_c^+ state is obtained by viewing the evolution of the complex amplitude in the Argand diagram[12]. In the amplitude fits discussed above, the $P_c(4450)^+$ is represented by a Breit-Wigner amplitude, where the magnitude and phase vary with $m_{J/\psi p}$ according to an approximately circular trajectory in the ($\mathrm{Re}A^{P_c}$, $\mathrm{Im}A^{P_c}$) plane, where A^{P_c} is the $m_{J/\psi p}$ dependent part of the $P_c(4450)^+$ amplitude. We perform an additional fit to the data using the reduced Λ^* model, in which we represent the $P_c(4450)^+$ amplitude as the combination of independent complex amplitudes at six equidistant points in the range $\pm\Gamma=39$ MeV around $M=4\,449.8$ MeV as determined in the default fit. Real and imaginary parts of the amplitude are interpolated in mass between the fitted points. The resulting Argand diagram, shown in Fig. 13(a), is consistent with a rapid counter-clockwise change of the $P_c(4450)^+$ phase when its magnitude reaches the maximum, a behavior characteristic of a resonance. A similar study for the wider state is shown in Fig. 13(b); although the fit does show a large phase change, the amplitude values are sensitive to the details of the Λ^* model and so this latter study is not conclusive.

2 Models of pentaquark structure

All models must explain the J^P of the two states not just one. They also should predict properties of other yet to be observed states: masses, widths, J^P's. There are many explanations of the P_c^+ states.

Let us start with tightly bound quarks ala Jaffe[14]. Early work[15-17] has been expanded upon recently use of diquark-diquark-antiquark models[18-23] and diquark-triquark model[24]. Here each pair of two quarks form a colored object along with the lone antiquark. The three colors then form a colorless state.

Weakly bound "molecules" of a baryon plus a

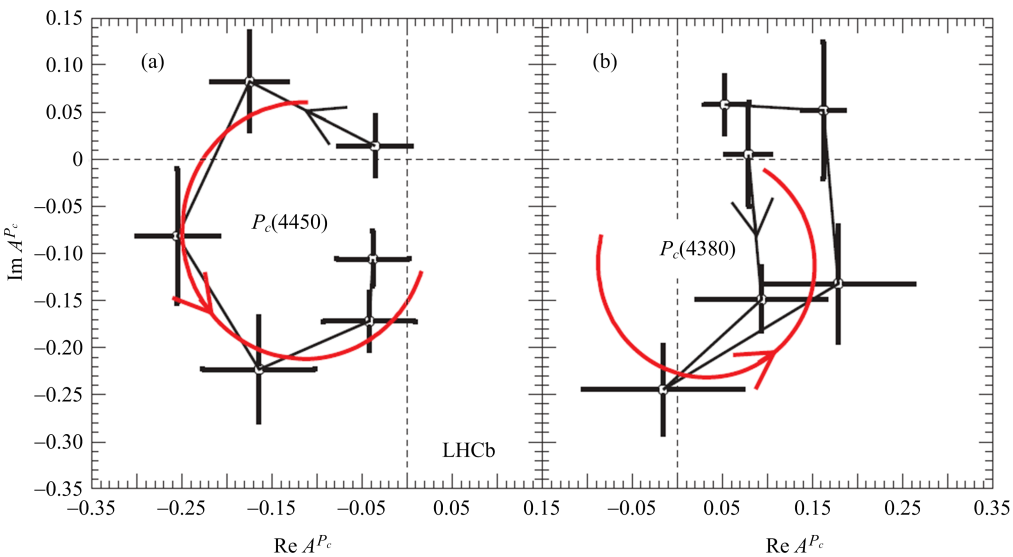

The solid (red) curves are the predictions from the Breit-Wigner formula. Systematic uncertainties are not included.

Fig. 13 Fitted values of the real and imaginary parts of the amplitudes for the baseline ($3/2^-$, $5/2^+$) fit for (a) the $P_c(4450)^+$ state and (b) the $P_c(4380)^+$ state, each divided into six $m_{J/\psi p}$ bins of equal width between $-\Gamma$ and $+\Gamma$ shown in the Argand diagrams as connected points with error bars ($m_{J/\psi p}$ increases counterclockwise)

meson, which are also built on previous work[25-30], have recently received much attention. Models trying to explain the states discussed here have already appeared[31-35], and even been disputed[36].

The $P_c(4450)^+$ is also explained by rescattering of $\chi_{c1}p \to J/\psi p$ as the sum masses of χ_{c1} and p is almost equal to the mass of this state[37-38].

3 Conclusion

After a half century of waiting, pentaquark states have been unmasked. Using a full amplitude fit to the $\Lambda_b^0 \to J/\psi K^- p$ decay, the LHCb collaboration has demonstrated two states of opposite parties decaying into $J/\psi p$, one having a mass of $(4380 \pm 8 \pm 29)$MeV and a width of $(205 \pm 18 \pm 86)$MeV, while the other has a mass of $(4\,449.8 \pm 1.7 \pm 2.5)$MeV and a width of $(39 \pm 5 \pm 19)$MeV. The parities of the two states are opposite with the preferred spins being 3/2 for one state and 5/2 for the other. The detailed binding mechanism of these states are subject to further studies. This work will lead to a better understanding of the strong interactions.

References

[1] GELL-MANN M. A schematic model of baryons and mesons[J]. Phys Lett, 1964,8:214-215.

[2] ZWEIG G. An SU3 model for strong interaction symmetry and its breaking: CERN-TH-401 [R]. [S. l.: s. n.], 1964.

[3] OLSEN S L. A new hadron spectroscopy[J]. Front Phys,2015,10:121-154.

[4] PILLONI A. XYZ: four-quark states? [EB/OL]. (2015-08-16) [2015-11-01]. http://arxiv.org/abs/1508.03823.

[5] AAIJ R, ADEVA B, ADINOLF M, et al. Observation of $J/\psi p$ resonances consistent with pentaquark states in $\Lambda_b^0 \to J/\psi K^- p$ decays[J]. Phys Rev Lett, 2015,115:072001.

[6] HICKS K H. On the conundrum of the pentaquark[J]. Eur Phys J H,2012,37(1): 1-31.

[7] AAIJ R, ADEVA B, ADINOLFI M, et al. Precision measurement of the ratio of the Λ_b^0 to $\overline{B}^0$ lifetimes[J]. Phys Lett B,2014,734:122-130.

[8] AAIJ R, ADEVA B, ADINOLFI M, et al. Precision measurement of the Λ_b^0 baryon lifetime[J]. Phys Rev Lett,2013,111:102003.

[9] ALVES JR A A, ANDRADE FILHO L M, BARBOSA A F, et al. The LHCb detector at the LHC [J/OL]. JINST, 2008, 3: S08005 [2015-11-01]. http://dx.doi.org/10.1088/1748-0221/3/08/S08005.

[10] HULSBERGEN W D. Decay chain fitting with a Kalman filter[J]. Nucl Instrum Meth A,2005,552:566-575.

[11] FLATTÉ S M. Coupled-channel analysis of the $\pi\eta$ and $K\overline{K}$ systems near $K\overline{K}$ threshold[J]. Phys Lett B, 1976,63: 224-227.

[12] OLIVE K A, AGASHE K, AMSLER C, et al. Review of particle physics [J]. Chin Phys C, 2014, 38(09): 090001.

[13] AAIJ R, ADEVA B, ADINOLFI M, et al. Study of the production of Λ_b^0 and $\overline{B}^0$ hadrons in pp collisions and first measurement of the $\Lambda_b^0 \to J/\psi p K^-$ branching fraction[EB/OL]. (2015-09-01)[2015-11-01]. http://arxiv.org/abs/1509.00292.

[14] JAFFE R J. Multiquark hadrons. I. Phenomenology of $Q^2\overline{Q}^2$ mesons[J]. Phys Rev D,1977, 15:267.

[15] STROTTMAN D. Multi-quark baryons and the MIT bag model[J]. Phys Rev D,1979,20: 748.

[16] HÄOGAASEN H, SORBA P. The systematics of possibly narrow quark states with baryon number one [J]. Nucl Phys B,1978,145(1): 119-140.

[17] Rossi G C, Veneziano G. A possible description of baryon dynamics in dual and gauge theories[J]. Nucl Phys B,1977,123(3):507-545.

[18] MAIANI L, POLOSA A D, RIQUER V. The new pentaquarks in the diquark model[J]. Phys Lett B, 2015,749:289-291.

[19] ANISOVICH V V, MATVEEV M A, NYIRI J, et al. Pentaquarks and resonances in the pJ/ψ spectrum [EB/OL]. (2015-07-28)[2015-11-01]. http://arxiv.org/abs/1507.07652.

[20] LI G N, HE M, HE X G. Some predictions of diquark model for hidden charm pentaquark discovered at the LHCb[EB/OL]. (2015-10-08)[2015-11-01]. http://arxiv.org/abs/1507.08252.

[21] GHOSH R, BHATTACHARYA A, CHAKRABARTI B. The masses of $P_c^*(4380)$ and $P_c^*(4450)$ in the quasi particle diquark model[J]. (2015-08-03)[2015-11-01]. http://arxiv.org/abs/1508.00356.

[22] WANG Z G. Analysis of the $P_c(4380)$ and $P_c(4450)$ as pentaquark states in the diquark model with QCD

sum rules[J]. (2015-08-03)[2015-11-01]. http://arxiv.org/abs/1508.01468.

[23] WANG Z G, HUANG T. Analysis of the $\frac{1}{2}^{\pm}$ pentaquark states in the diquark model with QCD sum rules[J]. (2015-08-18)[2015-11-01]. http://arxiv.org/abs/1508.04189.

[24] LEBED R F. The pentaquark candidates in the dynamical diquark picture[J]. Phys Lett B, 2015, 749: 454-457.

[25] VOLOSHIN M B, OKUN L B. Hadron molecules andcharmonium atom[J]. JETP Lett, 1976, 23: 333.

[26] DE RUJULA A, GEORGI H, GLASHOW S L. Molecular charmonium: a new spectroscopy? [J]. Phys Rev Lett, 1977, 38: 317

[27] TÄORNQVIST N A. Possible large deuteronlike meson-meson states bound by pions[J]. Phys Rev Lett, 1991, 67: 556.

[28] TÄORNQVIST N A. From the deuteron to deusons, an analysis of deuteronlike meson-meson bound states [J]. Z Phys C, 1994, 61 (3): 525-537.

[29] YANG Z C, SUN Z F, HE J, et al. The possible hidden-charm molecular baryons composed of anti-charmed meson and charmed baryon[J]. Chin Phys C, 2012, 36: 6-13.

[30] WANG W L, HUANG F, ZHANG Z Y, et al. $\Sigma_c\overline{D}$ and $\Lambda_c\overline{D}$ states in a chiral quark model[J]. Phys Rev C, 2011, 84: 015203.

[31] KARLINER M, ROSNERJ L. New exotic meson and baryon resonances from doubly-heavy hadronic molecules [EB/OL]. (2015-08-24)[2015-11-01]. http://arxiv.org/abs/1506.06386.

[32] ROCA L, NIEVES J, OSET E. The LHCb pentaquark as a $\overline{D}^*\Sigma_c - \overline{D}^*\Sigma_c^*$ molecular state[EB/OL]. (2015-10-21)[2015-11-01]. http://arxiv.org/abs/1507.04249.

[33] CHEN R, LIU X, LI X Q, et al. Identifying exotic hidden-charm pentaquarks [EB/OL]. (2015-08-29)[2015-11-01]. https://arxiv.org/abs/1507.03704.

[34] HE J. $\overline{D}\Sigma_c^*$ and $\overline{D}^*\Sigma_c$ interactions and the LHCb hidden-charmed pentaquarks [EB/OL]. (2015-07-18)[2015-11-01]. https://arxiv.org/abs/1507.05200.

[35] MEIßNER U G, OLLER J A. Testing the $\chi_{c1}p$ composite nature of the $P_c(4450)$[EB/OL]. (2015-08-25) [2015-11-01]. https://arxiv.org/abs/1507.07478.

[36] MIRONOV A, MOROZOV A. Is pentaquark doublet a hadronic molecule? [EB/OL]. (2015-07-16)[2015-11-01]. https://arxiv.org/abs/1507.04694.

[37] GUO F K, MEIßNER U G, WANG W, et al. How to reveal the exotic nature of the $P_c(4450)$[EB/OL]. (2015-10-22)[2015-11-01]. https://arxiv.org/abs/1507.04950.

[38] MIKHASENKO M. A triangle singularity and the LHCb pentaquarks[EB/OL]. (2015-07-23)[2015-11-01]. https://arxiv.org/abs/1507.06552.